hydrogen

MDPI

Article

Effect of Metal Carbides on Hydrogen Embrittlement: A Density Functional Theory Study

Omar Faye * and Jerzy A. Szpunar

Department of Mechanical Engineering, College of Engineering, University of Saskatchewan, 57 Campus Drive, Saskatoon, SK S7N 5A9, Canada; jerzy.szpunar@usask.ca
* Correspondence: omf071@usask.ca or omsofaye@yahoo.fr

Abstract: This study uses plane wave density functional theory (DFT) to investigate the effect of certain metal carbides (Niobium carbide, Vanadium carbide, Titanium carbide, and Manganese sulfide) on hydrogen embrittlement in pipeline steels. Our results predict that the interaction of hydrogen molecules with these metal carbides occurs in the long range with binding energy varying in the energy window [0.043 eV to 0.70 eV].In addition, our study shows the desorption of H_2 molecules from these metal carbides in the chemisorptions. Since atomic state hydrogen interacts with NbC, VC, TiC, and MnS to cause embrittlement, we classified the strength of the hydrogen trapping as TiC + H > VC + H > NbC + H> MnS + H. In addition, our study reveals that the carbon site is a more favorable hydrogen-trapping site than the metal one.

Keywords: hydrogen; embrittlement; niobium carbide; titanium carbide; vanadium carbide; manganese sulfide

check for updates

Citation: Faye, O.; Szpunar, J.A. Effect of Metal Carbides on Hydrogen Embrittlement: A Density Functional Theory Study. *Hydrogen* **2024**, *5*, 137–148. https://doi.org/10.3390/hydrogen5010009

Academic Editor: Jin-Yoo Suh

Received: 8 February 2024
Revised: 7 March 2024
Accepted: 18 March 2024
Published: 20 March 2024

1. Introduction

It is well known that high-strength steels are embrittled in a hydrogenous gas environment [1–4]. The key factors that favor hydrogen embrittlement are (i) the dissociation of hydrogen molecules, (ii) the diffusion of hydrogen atoms through the steel lattice along a preferential path such as the grain boundaries, or (iii) dislocation inducing plastic deformation at critical sites [5]. In addition, embrittlement of the material is enhanced by the decohesion of atomic layers at the interface or the recombination of hydrogen atoms at internal voids or defects [6]. Finally, there is a decrease in surface energy because of the adsorbed hydrogen or the hydride formation within certain alloys of vanadium, niobium, titanium, and zirconium [6]. Many theories about the factors that lead to this hydrogen embrittlement of steel are discussed in the literature [7]. Nahm et al. [8] reported that hydrogen embrittlement in pipeline steel provokes a delayed or sudden loss of ductility and reduces the load-bearing capability, even when the stress loading is far below the macroscopic yield points of the embrittled metallic materials. Liu et al. [9] stated that hydrogen dissolved in steel can lead to brittle fracture through segregation at crystal defects or accumulation at stress concentrations. It is reported that defects such as dislocations, grain boundaries, and inclusions can be used to alter hydrogen diffusion into the materials by trapping hydrogen at these defect sites [1]. It is also reported that using secondary phase particles as trapping sites can be an efficient way to improve the mechanical properties of steel by reducing the amount of diffusible hydrogen within the material [10]. Therefore, to promote the competitiveness of steel on the market, high-strength steels have been introduced that guarantee resistance against hydrogen embrittlement and stress corrosion cracking in various steel applications. Huang et al. [11] showed that a larger amount of the inclusions and a larger area and volume fraction of the inclusions make steels more susceptible to hydrogen-induced cracking. They also stated that steel with a microstructure consisting of granular bainite and martensitic/austenite microconstituents is more susceptible to

hydrogen-induced cracking [11]. In addition, to avoid the risk of deterioration in material strength, various researchers have pointed to the use of carbide precipitates formed above 500 °C as a feasible way to maintain the high strength of the steel even after applying a tempering process, as reported in the literature [7,12,13]. Balitskii et al. [14] studied hydrogen embrittlement in high-alloy chromium–nickel steels and alloys in hydrogen at high pressures and temperatures. They predicted that the mechanical characteristics of martensitic steels and nickel-base alloys are achieved at hydrogen pressures of over 10 and 30 MPa and of dispersion-hardening austenitic steels and alloys at a hydrogen content of 15 and 30 ppm, respectively [14]. In another study, they also stated that the influence of hydrogen on the morphology of fracture under static tension, crack resistance, and low-cycle fatigue testing is revealed within the temperature range of 293–473 K and under cyclic crack resistance testing over the temperature range of 293–673 K [15]. They showed that a decrease in the load frequency from 50 to 5 Hz leads to a decrease in the cyclic crack resistance threshold and contributes to significant crack acceleration in the presence of hydrogen in the middle section of kinetic fatigue fracture diagrams [16].

Several researchers have stated that employing a carbide precipitated phase as a hydrogen trap can enhance the resistance of steel to hydrogen embrittlement while generating more secondary cracks at the grain boundary [17,18]. Chen et al. [19] reported that increasing the number of carbon vacancies in individual metal carbides can enhance the hydrogen trapping capacity by introducing abundant metal carbides in steels.

Therefore, well-designed hydrogen trapping sites can improve the resistance of steel against hydrogen embrittlement (HE). In addition, it is well known that limited hydrogen diffusion may be sufficient to provoke a failure. Numerous studies have also found that the addition of microalloying elements (Nb, Ti, V, and Mo) might improve the HE resistance of steel [20]. In addition, metal carbide (MC) nanoprecipitates not only optimize the microstructure and improve the mechanical properties but also increase the hydrogen trap density in high-strength martensitic steels to improve HE resistance [16].

Buono et al. [20] studied the effect of nano NbC and VC carbides on the hydrogen interaction in tempered martensitic steels. They reported that the trapping capacity decreases in the following order: NbC > TiC > VC > MnS. Based on the existing research, this work aims to investigate the effects of metal carbide nanoprecipitates on the HE resistance of high-strength martensitic steels. Firstly, we studied the interaction of hydrogen molecules within the bulk structure of these metals.

Secondly, the interaction of the hydrogen atom and its preferential adsorption site was investigated.

Finally, the effect of layers of these carbides on hydrogen embrittlement was probed.

2. Computational Method

To model the hydrogen interaction with certain metal carbides including Niobium carbide (NbC), Titanium carbide (TiC), and Vanadium carbide (VC), we used the Dmol^{3}module implemented in material studio software (version 6.0) [14,21]. To approximate the exchange–correlation effect of electron–electron interaction, the Perdew–Wang exchange and correlation functional (PW91) was used [22]. Furthermore, the effect of a core electron as a single effective potential [23] was represented by using semicore pseudopotentials. The double numerical plus polarization (DNP) basis set was used as a basis set. To include the van der Waals interaction, we used the (DFT-D) scheme of Grimme et al. [24,25]. We used 225 as a space group number to model TiC and VC where Ti and V atoms occupy the origin positions (0, 0, 0), and C atoms are located in the (1/2, 0, 0) positions. NbC was also modeled with a space group number of 229 where Nb atoms occupy the origin positions (0, 0, 0) and C atoms are located in the (1/2, 0, 0) positions. Brillouin zone integration was performed through the Monkhorst–Packscheme [26] with a mesh grid of $2 \times 2 \times 2$. Energy minimization was performed with an energy convergence tolerance of 10^{-5} Ha. All atomic positions were relaxed such that the force on each atom was less than 0.002 Ha/Å. To improve the convergence, we used 0.25 Ha as a thermal smearing value.

3. Results and Discussion

3.1. Hydrogen Interaction with NbC, TiC, VC, and MnS Structures

Hydrogen embrittlement is a serious issue in the pipeline industry. Therefore, to mitigate this issue, many researchers use transition metal carbides as an alternative. In this study, we used Niobium carbide (NbC), Titanium carbide (TiC), Vanadium carbide (VC), and Manganese sulfide (MnS) to investigate their effect on hydrogen embrittlement. To begin with, we display the bulk structure of these under-investigated metal carbides in Figure 1.

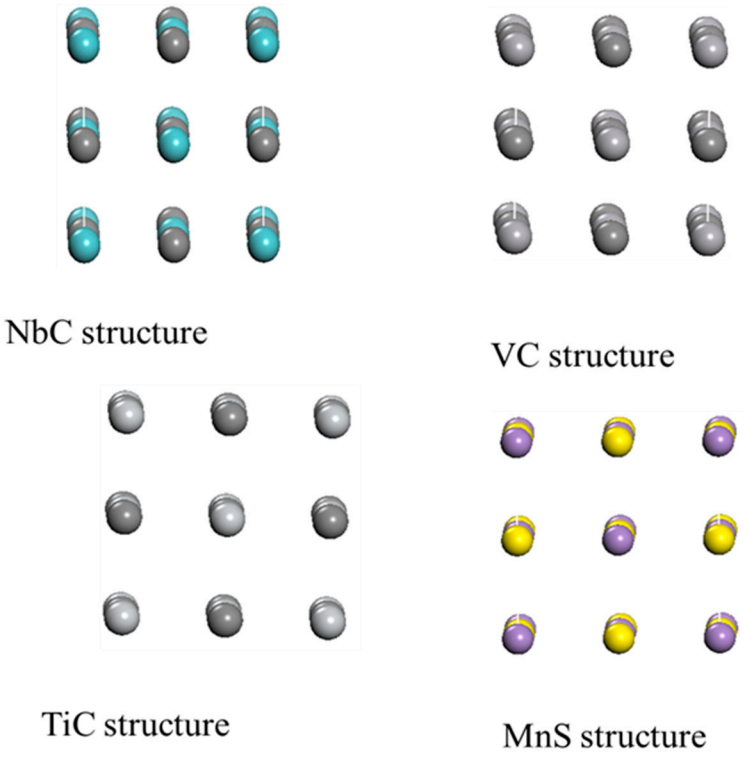

Figure 1. Schematic representation of Niobium carbide, Vanadium carbide, Titanium carbide, and Manganese sulfide. The green balls represent Niobium atoms (Nb), the gray ones stand for carbon (C), the slightly gray onesrepresent vanadium (V), the light gray ones represent titanium atoms (Ti), the yellow balls stand for sulfide(S), and the purple ones stand for manganese atoms (Mn).

The calculated bulk properties such as the lattice parameter and the band gap energy are listed in Table 1.

Table 1. Lattice parameter and band gap energy of Niobium carbide, Vanadium carbide, Titanium carbide, and Manganese sulfide.

Metal Carbide	Lattice Parameter (Å)	Energy Band Gap E_g (eV)
NbC	4.40	0.006
VC	4.18	0.007
TiC	4.36	0.09
MnS	5.70	3.2

Table 1 shows that the calculated lattice parameter of Niobium carbide (NbC) is 4.40 Å compared to 4.51 Å [27] and 4.43 Å [28,29], as reported in the literature. Also, as indicated in Table 1, the calculated lattice parameter of Vanadium carbide is 4.18 Å compared to the experimental value of4.16 Å [30,31], and the calculated lattice parameter of Titanium carbide is 4.36 Å compared to its experimental value of 4.32 Å [32–34]. Finally, the calculated

lattice parameter of Manganese sulfide is 5.07 Å compared to its experimental value of 5.60 Å [35]. The good agreement between the theoretical and experimental values and, also, the small deviation between the experimental and theoretical values show that our approximation to model these structures is reliable. Furthermore, we studied the chemical stability of these metal carbides by determining the energy band gap using Equation (1).

$$E_g = E_{LUMO} - E_{HOMO} \quad (1)$$

where E_{LUMO} is the energy of the lowest unoccupied molecular orbital (LUMO) and E_{HOMO} is the energy of the highest occupied molecular orbital (HOMO).

A vacuum space of 15 Å was created in order to avoid the image interaction and to accurately model the adsorption of the metal carbides with hydrogen.

The calculated energy band gap of Niobium carbide crystal is 0.04 eV, which is slightly deviated from the zero gap reported by Delgado et al. [36]. In the same trend, Lin et al. [37] stated that Vanadium carbide has good metal properties, which is in good agreement with our energy band gap calculation (E_g) of 0.007 eV. Also, Mohsen et al. [32] predicted similar characteristics for Titanium carbide with a zero-band gap energy compared to our computed value of 0.09 eV. This contrasts with Manganese sulfide (MnS), where the experimental value of the energy band gap is 3 eV [35,38] compared with our calculated value of 3.2 eV.

Moreover, knowing their lattice parameters and their chemical stability, we further studied the two most common ways that molecular hydrogen interacts with the metal carbides (physisorption and chemisorption).

Firstly, we studied the interaction of hydrogen molecules in their physisorption interaction with Niobium carbide (NbC), Titanium carbide (TiC), Vanadium carbide (VC) and Manganese sulfide (MnS). The initial and optimized structures in the physisorption interaction of hydrogen with these metal carbides are shown in Figure 2.

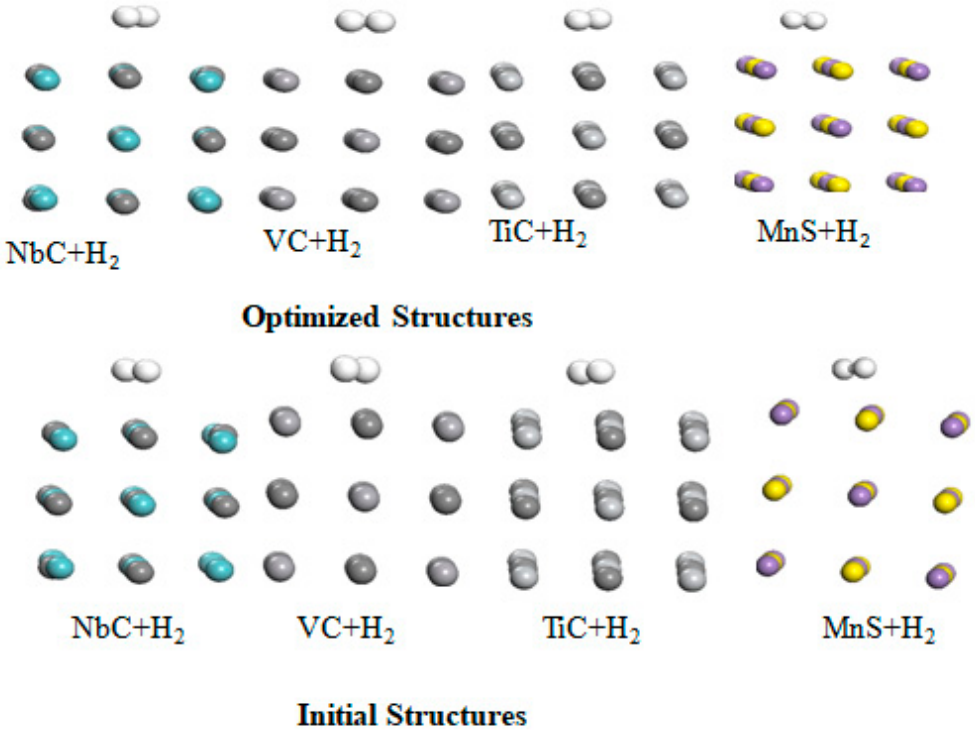

Figure 2. The initial and final structures of the interaction betweenhydrogen molecules andNbC, TiC, VC, and MnS. The green balls represent niobium atoms (Nb), the gray ones stand for carbon (C), the slightly gray ones are vanadium (V), the light gray ones stand for titanium atoms (Ti), the yellow balls stand for sulfide, the white balls represent hydrogen atoms (H), and the purple ones stand for manganese atoms (Mn).

We evaluated the strength of the interaction of each H_2 molecule with the studied metal carbides using the Equation (2):

$$E_b = E_{(MC)} + E_{(H)} - E_{(MC+H)} \quad (2)$$

where $E_{(MC)}$ stands for the total energy of the metal carbide in its primitive unit cell, $E_{(H)}$ is the ground energy of a hydrogen molecule in a cubic cell of the lattice parameter (a = 20 Å), and $E_{(MC+H)}$ is the total energy of the metal carbide plus the H_2 molecule.

The calculated binding energy along with the equilibrium distance of the optimized structures are summarized in Table 2.

Table 2. Adsorption energy of hydrogen molecules with Niobium carbide, Titanium carbide, Vanadium carbide, and Manganese carbide.

Metal Carbide +H_2 Molecule	Adsorption Energy E_b (eV)	d_{eq} (Å)
NbC + H_2	0.050	1.417
TiC + H_2	0.70	1.204
VC + H_2	0.62	1.309
MnS + H_2	0.043	1.810

Table 2 reveals that the binding energy between hydrogen molecules and the metal carbides in the physisorption case are van der Waal interactions, where the adsorption energy ranges from 0.043 eV to 0.70 eV. In addition, their equilibrium distances range from 1.204 Å to 1.810 Å, which were determined from their optimized structure as displayed in Figure 2. These calculated results align with earlier results reported in the literature [1,39,40].

Furthermore, we investigated the interaction of hydrogen with the precipitate in the presence of steel. To do so, Fe crystal was cleaved alongthe {111}, {110}, and {100} surfaces. After calculation, the Fe {110} surface was identified to have the most stability compared with the other Fe surfaces. Therefore, the Fe{110} surface was selected to study the interaction of hydrogen molecules sandwiched between its surface and the four precipitates (NbC, TiC, VC, and MnS). The initial and optimized structures of this interaction are displayed in Figure 3.

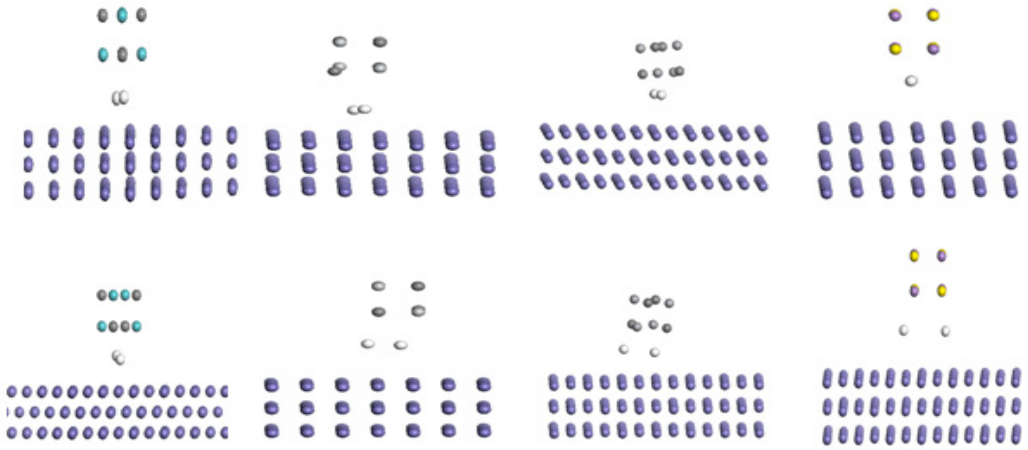

Figure 3. The initial and final structures of the interaction of hydrogen molecules sandwiched between an Fe{110} surface and NbC, TiC, VC, and MnS. The green balls represent niobium atoms (Nb), the gray ones stand for carbons (C), the slightly gray ones are vanadium (V), the light gray ones represent titanium atoms (Ti), the yellow balls stand for sulfide, the white balls stand for hydrogen atoms (H), and the purple ones stand for manganese atoms (Mn).

Figure 3 reveals the total dissociation of the H_2 molecules in all cases. The binding energies and the equilibrium distances of H_2 between Fe {110} and the precipitates are summarized in Table 3. Initially, we placed each H_2 molecule at a distance of 2.6 Å with respect to Fe{110} and 2.8 Å with respect to the precipitate atom.

Table 3. A summary of the equilibrium parameters such as binding energy (E_b (eV)) and the optimized distance of the hydrogen atom with respect to the Fe atom and H atom (d_{eq} (Å)).

Fe(110) + Metal Carbide +H_2 Molecule	Adsorption Energy E_b (eV)	d_{eq} (Å)	d_{eq}(Å)
Fe(110) + NbC + H_2	0.320	2.63	2.38
Fe(110) + TiC + H_2	0.570	3.64	2.42
Fe(110) + VC + H_2	0.42	2.68	2.52
Fe(110) + MnS + H_2	0.13	3.21	2.89

The equilibrium distances between the hydrogen atoms and the closest top atoms of the Fe {110} surface fall in the interval [2.6 to 3.21 Å], while the interval is [2.38 to 2.65 Å] in the cases of the precipitates, as shown in Table 3. From our results, we can state that the presence of the Fe surface favors the dissociation of the H_2 molecule. Also, the dissociated hydrogen molecule is closer to the precipitate atoms than the Fe {110} surface.

Furthermore, we investigated the interaction of H_2 in the chemisorptions case with the aforementioned metal carbides. The initial and optimized structures of these complexes are portrayed in Figure 4 to better visualize this interaction.

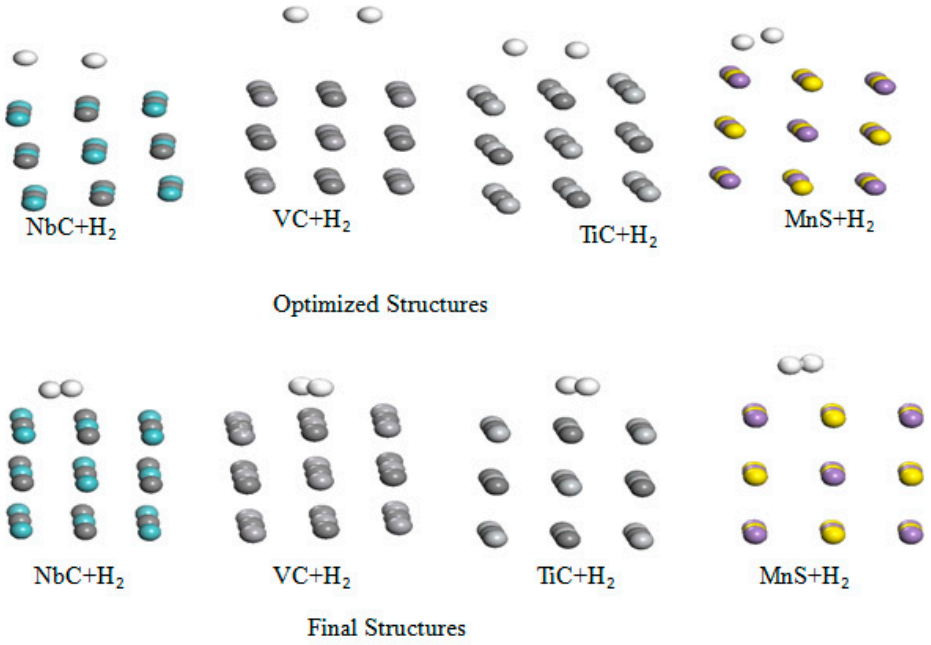

Figure 4. Initial and optimized structures of Niobium carbide (NbC), Titanium carbide (TiC), Vanadium carbide (VC), and Manganese sulfide (MnS). The green balls represent niobium atoms (Nb), the gray ones stand for carbons (C), the slightly gray ones are vanadium (V), the light gray ones stand for titanium atoms (Ti), the yellow balls stand for sulfide, the white balls represent hydrogen atoms (H), and the purple ones stand for manganese atoms (Mn).

Our calculations reveal that spontaneous dissociation of the H_2 molecule occurs in all cases in the chemisorptions of hydrogen with the metal carbides, as shown in Figure 3. This result aligns with the earlier result of Silveri et al. [39], where a spontaneous dissociative chemisorption was observed to happen when the molecule was placed less than 2.0 Å

above the topmost surface atomic plane. To better visualize these results, the equilibrium parameters such as binding energy (E_b) and the optimized distance of hydrogen with the matrix (d_{eq}) are summarized in Table 4.

Table 4. Summary of the final parameters such as binding energy (E_b) and equilibrium distance (d_{eq}).

Metal Carbide	Adsorption Energy E_b (eV)	d_{eq} (Å)
NbC	0.39 eV	2.04
VC	0.59 eV	1.867
TiC	0.63 eV	1.678
MnS	0.46 eV	1.89

From Table 4, the strength of hydrogen trapping can be arranged in the following order: TiC + H_2 > VC + H_2 > MnS + H_2 > NbC + H_2, and the equilibrium distance varies in this interval: [1.67 Å to 2.04 Å]. According to the literature, the trapping of hydrogen can be generally classified as strong or weak. Weak trapping occurs when the binding energy is less than 0.31 eV (30 KJmol), while strong trapping happens when the trapping energy is greater than 0.63 eV (60 KJ/mol) [1].These results predict that all the metal carbides have strong hydrogen trapping: the binding energies with hydrogen molecules are all greater than 0.63 eV. Therefore, NbC, TiC, and VC are potential precipitates to enhance the strength of steel due to their strong hydrogen trapping energy. Hydrogen embrittlement occurs essentially in the atomic state of hydrogen; therefore, in the next section, we investigate the interaction of hydrogen atoms with the studied metal carbides.

3.2. Interaction of the Metal Carbides (NbC, TiC, VC, and MnS) with Hydrogen Atoms

Hydrogen from two types of sources can interact with metal as follows: hydrogen generated at the metal surface and gaseous hydrogen. In a gaseous state, it is in the molecular form at standard conditions; therefore, it does not produce embrittlement. However, atomic hydrogen creates embrittlement because it dissolves rapidly into metal at room temperature [41]. Therefore, to have more insight into the hydrogen embrittlement of the studied carbides, we investigated their interaction with hydrogen atoms. To do so, we created two layers of bulk crystal separated by a vacuum of 15 Å with another 15 Å vacuum for the top layer in order to avoid the strong interaction between these layers.

We displayed the initial and optimized structures of this interaction in Figure 5.

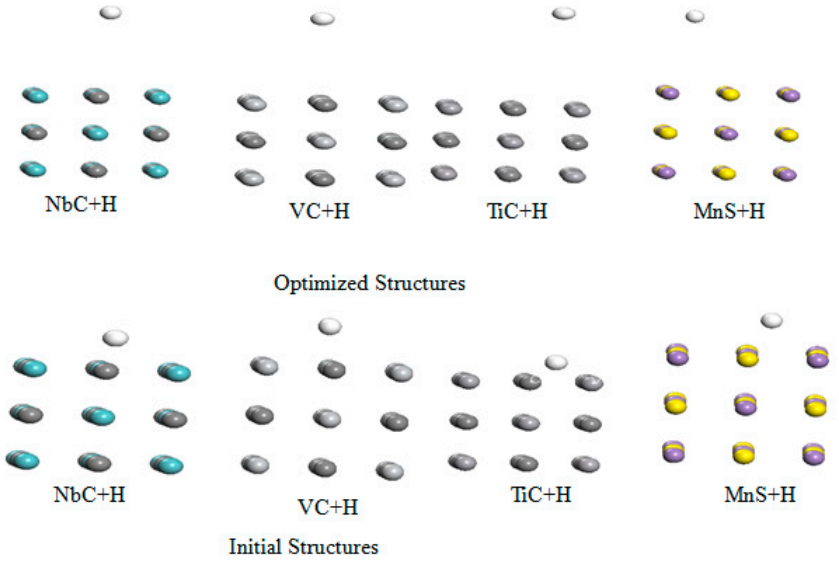

Figure 5. Representation of the initial and final structures of the interaction of hydrogen atoms with NbC, VC, TiC, and MnS.

We summarized the optimized parameters for these structures such as binding energy (E_b) and final distance between the hydrogen atom and the studied metal carbides (d_{eq}) in Table 5.

Table 5. Summary of the adsorption energy and the optimized distance of hydrogen with NbC, VC, TiC, and MnS.

Metal Carbide +H_2 Molecule	Adsorption Energy E_b (eV)	d_{eq} (Å)
NbC + H	0.240	1.94
VC + H	0.48	1.78
TiC + H	0.840	1.13
MnS + H	0.127	2.08

Table 5 reveals that the most favorable trap site for hydrogen atoms among the metal carbides is TiC with E_b = 0.840 eV, followed by VC with E_b = 0.480 eV, NbC with E_b = 0.240 eV, and MnS with E_b = 0.127 eV. In addition, their corresponding equilibrium distances (d_{eq}) range in the interval [1.13 Å, 2.08 Å]. Moreover, we studied the most favorable adsorption site between the metal and the carbon atom in the metal carbides. To do so, we chemisorbed the hydrogen atom on the carbon and metal sites successively and determined the binding energy on these sites using Equation (1).

The adsorption energies (E_b) and the corresponding final distances (d_f) of hydrogen atoms within the metal carbides are summarized in Table 6.

Table 6. Summary of the optimized parameters such as binding energy and the final distance between the hydrogen atom and the adsorption site.

Metal Carbide	Adsorption Energy Site	Adsorption Energy (eV)	Final Distance (d_f) (Å)
NbC	C	1.22	1.14
	Nb	0.96	1.50
VC	C	1.33	1.14
	V	1.03	1.29
TiC	C	1.55	1.14
	Ti	1.04	1.862
MnS	Mn	0.88	1.73
	S	1.28	1.65

From Table 6, we learned that the most favorable adsorption occurs at the carbon site in NbC, VC, and TiC with binding energy lying in the energy window [1.22 eV, 1.55 eV]. The binding energy of the metal sites (Nb, V, and Ti) varied in this interval [0.96 eV, 1.04 eV]. However, for manganese sulfide (MnS), the most favorable trapping site is the sulfur atom with E_b = 1.28 eV compared with E_b = 0.88 eV for the manganese atom (Mn). These results follow the trend in earlier results reported in the literature [20,39]. In the last section, we discuss the effect of the layer on the trapping capacity of the carbides.

3.3. The Effect of theLayer on Hydrogen Interactions with NbC, TiC, VC, and MnS

Understanding the interactions of H_2 molecules and hydrogen atoms helped us to choose a new direction for this research. In this section, we investigated the effect of the layer on the hydrogen embrittlement in Niobium carbide, Titanium carbide, Vanadium carbide, and Manganese sulfide. Firstly, we used two layers with a vacuum spacing of 15 Å. The initial and optimized structures of the metal carbides are shown in Figure 6 below.

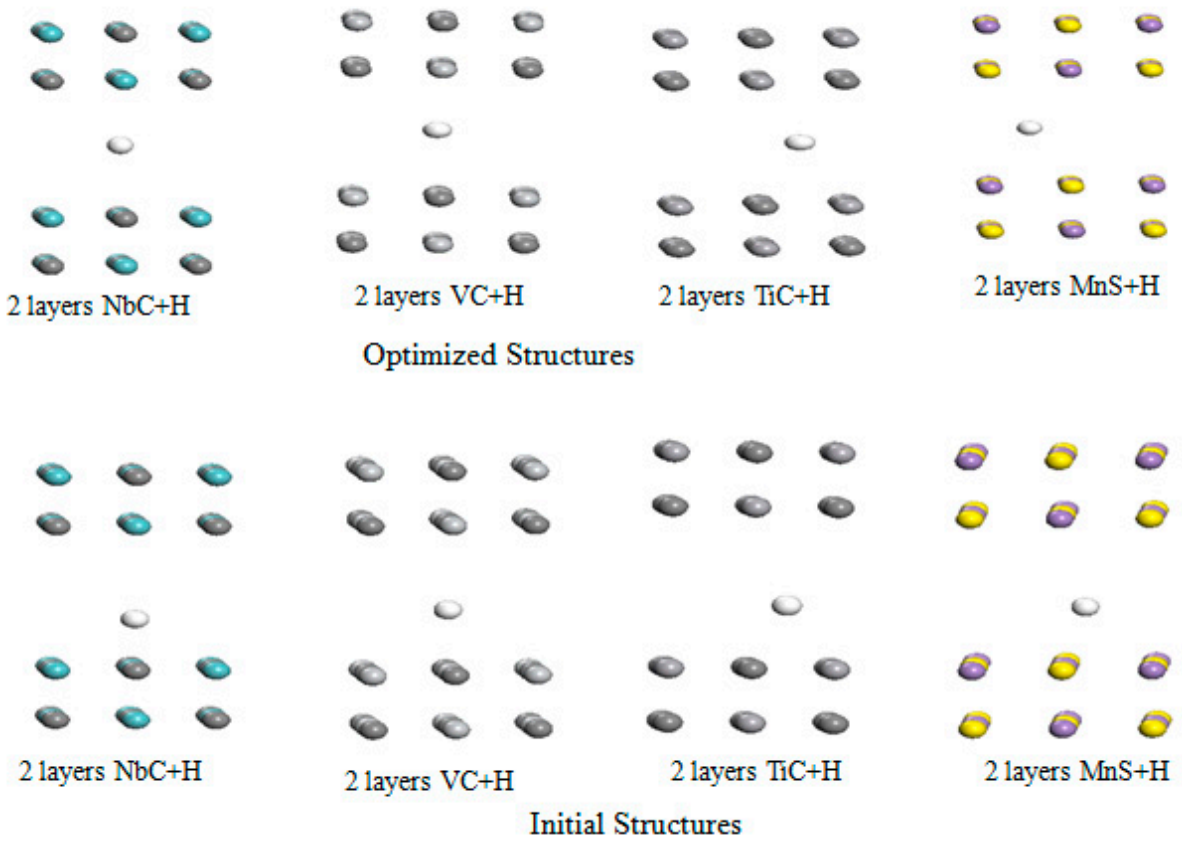

Figure 6. The initial and optimized structures of Niobium carbide, Titanium carbide, Vanadium carbide, and Manganese sulfide.

Furthermore, we determined the strength of the interaction of hydrogen atoms with the two layers of NbC, TiC, VC, and MnS using Equation (2).

The optimized parameters such as the binding energy of hydrogen atoms with the metal carbides are summarized in Table 7.

Table 7. Summary of the adsorption energy of NbC, VC, TiC, and MnS along the energy band.

Metal Carbide	Adsorption Energy E_b (eV)	d_{eq} (Å)
NbC	0.34	1.65
VC	0.52	1.45
TiC	0.88	1.24
MnS	0.21	1.76

Table 7 reveals that the adsorption energy is in the energy window of 0.21 eV to 0.88 eV. The binding of the H atom is more favorable in the case of the NbC layer. In addition, their optimized distance is between 1.24 Å to 1.76 Å. We noticed a slight increase in the binding energy of hydrogen atoms in these carbides. Furthermore, we increased the number of layers from two to three for all the carbides. The initial and optimized structures in this interaction are shown in Figure 7.

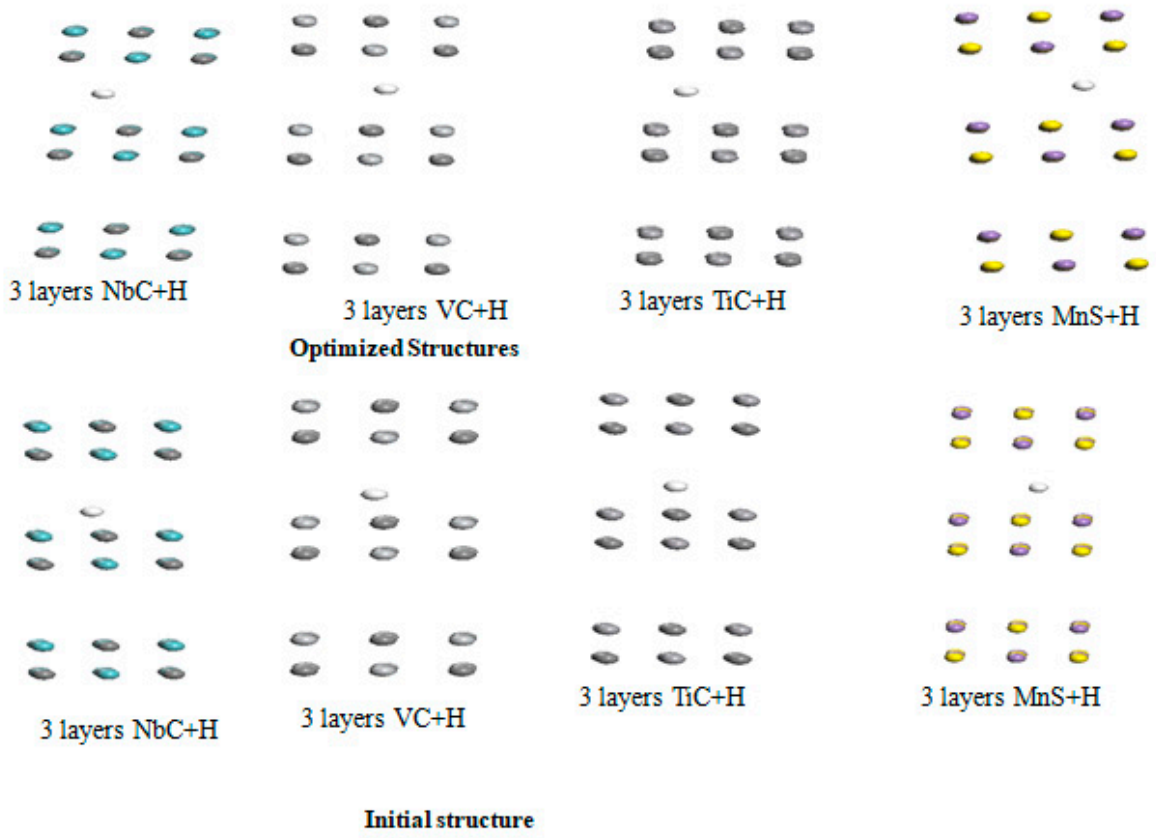

Figure 7. Initial and optimized structures of the interaction of hydrogen with three layers of bulk NbC, VC, TiC, and MnS.

Moreover, we summarized in Table 8 the resulting parameters like adsorption energy and equilibrium distance for the interaction between hydrogen atoms and the carbides under study.

Table 8. Summary of the adsorption energies of NbC, VC, TiC, and MnS along with their equilibrium distances.

Metal Carbide	Adsorption Energy E_b (eV)	d_{eq} (Å)
2NbC + H	0.34	1.78
2VC + H	0.56	1.45
2TiC + H	0.93	1.32
2MnS + H	0.28	1.87

Table 8 shows increased adsorption energy with an increased number of layers, proving that this can also be an efficient way to enhance the trapping of hydrogen on the studiedcarbides.

4. Conclusions

We used plane-wave density functional theory to study the interaction of hydrogen with some metal carbides such as Niobium carbide (NbC), Titanium carbide (TiC), Vanadium carbide (VC), and Manganese sulfide (MnS). Our results suggest that the interaction of molecular hydrogen with these metal carbides happens in the gas phase with a binding energy in the energy window [0.70 eV to 0.043 eV]. Our results also predict that H_2 desorbs from these metals during chemisorption. Since hydrogen embrittlement occurs in the atomic state of hydrogen, our finding shows that the strength of the trapping of hydrogen

atoms can be classified as TiC + H > VC + H > NbC + H > MnS + H. In addition, our study reveals that the carbon site is a more favorable hydrogen-trapping site than the metal one. Also, we can state that the presence of the Fe surface favors the dissociation of the H_2 molecule, and the dissociated hydrogen molecule is closer to the precipitate atoms than the Fe {110} surface.

Furthermore, our results also demonstrate that increasing the number of layers can also be an efficient way to enhance the trapping capacity. Our findings highlight the important role of carbon vacancies in transition metal carbides for a remarkable increase in hydrogen trapping capacity.

Author Contributions: O.F. is the main investigator of this research. J.A.S. is the principal supervisor of this research. All authors have read and agreed to the published version of this manuscript.

Funding: This research received no external funding.

Data Availability Statement: All data and materials are available on request from the corresponding author. The data are not publicly available due to ongoing researches using a part of the data.

Acknowledgments: We acknowledge access to high-performance supercomputers, Compute Canada, and Plato at the University of Saskatchewan. This work was supported by the National Engineering Research Council of Canada and the Canada Research Chairs program.

Conflicts of Interest: The authors declare no competing financial interests.

References

1. Salehin, R.; Thompson, G.B.; Weinberger, C.R. Hydrogen trapping and storage in the group IVB-VIB transition metal carbides. *Mater. Des.* **2022**, *214*, 110399. [CrossRef]
2. Wasim, M.; Djukic, M.B. Hydrogen embrittlement of low carbon structural steel at macro-, micro- and nano-levels. *Int. J. Hydrogen Energy* **2020**, *45*, 2145–2156. [CrossRef]
3. Zhou, X.; Tehranchi, A.; Curtin, W.A. Mechanism and Prediction of Hydrogen Embrittlement in fcc Stainless Steels and High Entropy Alloys. *Phys. Rev. Lett.* **2021**, *127*, 175501. [CrossRef] [PubMed]
4. Tkachov, V.I.; Ivas'kevych, L.M.; Voznychak, O.M. Degradation of steel in gaseous hydrogen with inhibiting admixtures. *Mater. Sci.* **2007**, *43*, 377–382. [CrossRef]
5. Neikter, M.; Colliander, M.; Schwerz, C.d.A.; Hansson, T.; Åkerfeldt, P.; Pederson, R.; Antti, M.-L. Fatigue crack growth of electron beam melted TI-6AL-4V in high-pressure hydrogen. *Materials* **2020**, *13*, 1287. [CrossRef] [PubMed]
6. Schaper, M.K. Fatigue crack closure at near-threshold growth rates in steels, effects of microstructure, load sequence and environment. *J. ASTM Int.* **2012**, *9*, 1–17. [CrossRef]
7. Wang, Y.; Wang, X.; Gong, J.; Shen, L.; Dong, W. Hydrogen embrittlement of catholically hydrogen-precharged 304L austenitic stainless steel: Effect of plastic pre-strain. *Int. J. Hydrogen Energy* **2014**, *39*, 13909–13918. [CrossRef]
8. Nguyen, T.T.; Park, J.S.; Kim, W.S.; Nahm, S.H.; Beak, U.B. Environment hydrogen embrittlement of pipeline steel X70 under various gas mixture conditions with in situ small punch tests. *Mater. Sci. Eng. A* **2020**, *781*, 139114. [CrossRef]
9. Lin, L.; Li, B.-S.; Zhu, G.-M.; Kang, Y.-L.; Liu, R.-D. Effect of niobium precipitation behavior on microstructure and hydrogen induced cracking of press hardening steel 22MnB5. *Mater. Sci. Eng. A* **2018**, *721*, 38–46. [CrossRef]
10. Nagao, A.; Martin, M.L.; Dadfarnia, M.; Sofronis, P.; Robertson, I.M. The effect of nanosized (Ti,Mo)C precipitates on hydrogen embrittlement of tempered lath martensitic steel. *Acta Mater.* **2014**, *74*, 244–254. [CrossRef]
11. Huang, F.; Liu, J.; Deng, Z.J.; Cheng, J.H.; Lu, Z.H.; Li, X.G. Effect of microstructure and inclusions on hydrogen induced cracking susceptibility and hydrogen trapping efficiency of X120 pipeline steel. *Mater. Sci. Eng. A* **2010**, *527*, 6997–7001. [CrossRef]
12. Peral, L.B.; Zafra, A.; Fernández-Pariente, I.; Rodríguez, C.; Belzunce, J. Effect of internal hydrogen on the tensile properties of different CrMo(V) steel grades: Influence of vanadium addition on hydrogen trapping and diffusion. *Int. J. Hydrogen Energy* **2020**, *45*, 22054–22079. [CrossRef]
13. Peral, L.B.; Fernández-Pariente, I.; Colombo, C.; Rodríguez, C.; Belzunce, J. The positive role of nanometric molybdenum–vanadium carbides in mitigating hydrogen embrittlement in structural steels. *Materials* **2021**, *14*, 7269. [CrossRef] [PubMed]
14. . . . Materials Studio. *Chem. Eng. News Arch.* **2000**, *78*, ibc. [CrossRef]
15. Balyts'kyi, O.I.; Ivas'kevych, L.M.; Mochul's'kyi, V.M. Mechanical properties of martensitic steels in gaseous hydrogen. *Strength Mater.* **2012**, *44*, 64–71. [CrossRef]
16. Balyts'kyi, O.I.; Ivas'kevych, L.M. Load Rate-Related Mechanical Properties of Steels and Alloys under Static and Cyclic Loading in Gaseous Hydrogen. *Strength Mater.* **2021**, *53*, 430–439. [CrossRef]
17. Depover, T.; Verbeken, K. The effect of TiC on the hydrogen induced ductility loss and trapping behavior of Fe-C-Ti alloys. *Corros. Sci.* **2016**, *112*, 308–326. [CrossRef]
18. Lawrence, S.K.; Wharry, J.P. Hydrogen Effects on Material Performance. *JOM* **2020**, *72*, 1979–1981. [CrossRef]

19. Liu, P.-Y.; Zhang, B.; Niu, R.; Lu, S.-L.; Huang, C.; Wang, M.; Tian, F.; Mao, Y.; Li, T.; Burr, P.A.; et al. Engineering metal-carbide hydrogen traps in steels. *Nat. Commun.* **2024**, *15*, 724. [CrossRef] [PubMed]
20. dos Santos, T.A.A.; de Lima, M.M.; dos Santos, D.S.; Buono, V.T.L. Effect of nano Nb and V carbides on the hydrogen interaction in tempered martensitic steels. *Int. J. Hydrogen Energy* **2022**, *47*, 1358–1370. [CrossRef]
21. Delley, B. From molecules to solids with the DMol^3 approach. *J. Chem. Phys.* **2000**, *113*, 7756–7764. [CrossRef]
22. Perdew, J.P.; Burke, K.; Ernzerhof, M. Generalized gradient approximation made simple. *Phys. Rev. Lett.* **1996**, *77*, 3865–3868. [CrossRef]
23. Perdew, J.P.; Chevary, J.A.; Vosko, S.H.; Jackson, K.A.; Pederson, M.R.; Singh, D.J.; Fiolhais, C. Applications of the generalized gradient approximation for exchange and correlation. *Phys. Rev. B* **1992**, *46*, 6671. [CrossRef]
24. Grimme, S.; Antony, J.; Ehrlich, S.; Krieg, H. A consistent and accurate ab initio parametrization of density functional dispersion correction (DFT-D) for the 94 elements H-Pu. *J. Chem. Phys.* **2010**, *132*, 154104–154119. [CrossRef]
25. Faye, O.; Eduok, U.; Szpunar, J.A. Boron-Decorated Graphitic Carbon Nitride (g-C_3N_4): An Efficient Sensor for H_2S, SO_2, and NH_3 Capture. *J. Phys. Chem. C* **2019**, *123*, 29513–29523. [CrossRef]
26. Wang, Y.; Wisesa, P.; Balasubramanian, A.; Dwaraknath, S.; Mueller, T. Rapid generation of optimal generalized Monkhorst-Pack grids. *Comput. Mater. Sci.* **2021**, *187*, 110100. [CrossRef]
27. Connétable, D. First-principles study of transition metal carbides. *Mater. Res. Express* **2016**, *3*, 126502. [CrossRef]
28. Hugosson, H.W.; Jansson, U.; Johansson, B.; Eriksson, O. Phase stability diagrams of transition metal carbides, a theoretical study. *Chem. Phys. Lett.* **2001**, *333*, 444–450. [CrossRef]
29. Sun, S.; Fu, H.; Lin, J.; Guo, G.; Lei, Y.; Wang, R. The stability, mechanical properties, electronic structures and thermodynamic properties of (Ti, Nb)C compounds by first-principles calculations. *J. Mater. Res.* **2018**, *33*, 495–506. [CrossRef]
30. Liu, F.; Yao, Y.; Zhang, H.; Kang, Y.; Yin, G.; Huang, Z.; Liao, X.; Liang, X. Synthesis and characterization of vanadium carbide nanoparticles by thermal refluxing-derived precursors. *J. Mater. Sci.* **2011**, *46*, 3693–3697. [CrossRef]
31. Liu, Y.; Huang, S.; Ding, J.; Yang, Y.; Zhao, J. Vanadium carbide coating as hydrogen permeation barrier: A DFT study. *Int. J. Hydrogen Energy* **2019**, *44*, 6093–6102. [CrossRef]
32. Mhadhbi, M.; Driss, M. Titanium Carbide: Synthesis, Properties and Applications. *Brill. Eng.* **2020**, *2*, 1–11. [CrossRef]
33. Xiong, H.; Zhang, H.; Zhang, H.; Gan, L. First Principle Calculation of NbC Precipitation Competition between TiC Particle and Ferrite Matrix. *J. Wuhan Univ. Technol. Mater. Sci. Ed.* **2018**, *33*, 1076–1081. [CrossRef]
34. Yang, Y.; Lu, H.; Yu, C.; Chen, J.M. First-principles calculations of mechanical properties of TiC and TiN. *J. Alloys Compd.* **2009**, *485*, 542–547. [CrossRef]
35. Ferretti, A.M.; Mondini, S.; Ponti, A. Manganese Sulfide (MnS) Nanocrystals: Synthesis, Properties, and Applications. *Adv. Colloid Sci.* **2016**, 121–123. [CrossRef]
36. Delgado, N.; Salas, O.; Garcés, E.; Magaña, L.F. Ab-Initio Calculation of the Electrical Conductivity, Optical Absorption, and Reflectivity of the 2D Materials SnC and NbC. *Crystals* **2023**, *13*, 682. [CrossRef]
37. Lin, L.; Yang, X.; Shi, P.; Yan, L.; Xie, K.; Deng, C.; Chen, Z. Probing the origin of transition metal carbide VC for oxygen reduction reaction: A DFT study. *Surf. Interfaces* **2023**, *40*, 103100. [CrossRef]
38. Hansa; Sahani, S.; Kim, T.Y. Metal Nanocomposites for Energy and Environmental Applications. *Energy Environ. Sustain.* **2022**, 293–318. [CrossRef]
39. Silveri, F.; Quesne, M.G.; Roldan, A.; de Leeuw, N.H.; Catlow, C.R.A. Hydrogen adsorption on transition metal carbides: A DFT study. *Phys. Chem. Chem. Phys.* **2019**, *21*, 5335–5343. [CrossRef]
40. Vandewalle, L.; Depover, T.; Verbeken, K. Hydrogen trapping of carbides during high temperature gaseous hydrogenation. *Int. J. Hydrogen Energy* **2023**, *48*, 32158–32168. [CrossRef]
41. Song, J.; Curtin, W.A. Atomic mechanism and prediction of hydrogen embrittlement in iron. *Nat. Mater.* **2013**, *12*, 145–151. [CrossRef] [PubMed]